

Supersolid spectroscopy

L. M. Platt¹, D. Baillie², and P. B. Blakie¹

¹*Dodd-Walls Centre for Photonic and Quantum Technologies, Dunedin 9054, New Zealand*

²*Department of Physics, University of Otago, Dunedin 9016, New Zealand*

(Dated: December 23, 2024)

We develop a linear response theory to provide a unified description of two recent spectroscopy protocols for probing one-dimensional supersolid states realized in cold-atom systems. Both protocols involve applying a periodic optical potential to excite the supersolid and determine its excitation frequencies and density response characteristics. This information can be used to estimate the superfluid fraction. We validate our linear response theory against nonlinear meanfield simulations of the dynamics for both translationally invariant and trapped cases. A key focus is the behavior at the band edge - the regime occurring when the optical potential used to excite the system has a wavelength that is twice the value of the supersolid lattice constant. Here symmetry can be used to selectively excite a mode from one of the two low-energy gapless excitation bands. Finally, we consider the application of the spectroscopy protocols to determine the superfluid fraction, showing the relationship to hydrodynamic theory and a Josephson-Junction array model.

I. INTRODUCTION

Recently Šindik *et al.* [1] proposed a protocol for probing a supersolid state of a dipolar Bose Einstein condensate (BEC) by abruptly removing an applied spatially periodic potential. The resulting oscillations of the supersolid exhibited two frequency components that they related to the quasiparticle excitation energy and static density response function of the lowest two bands at the wavelength set by the perturbation. For long-wavelength perturbations the lowest two excitation bands are well-described by hydrodynamic theory, and this protocol can be used to determine the compressibility, the elastic modulus of the lattice, and the superfluidity.

Another protocol has been developed and applied to an experiment with a dipolar supersolid by Biagioni *et al.* [2]. This involved the brief application of a strong periodic potential, with a period of two lattice sites, to imprint a differential phase between adjacent sites. The subsequent dynamics revealed a Josephson Junction-like oscillation involving the phase difference and atom number difference between adjacent sites. This protocol was used to provide direct evidence of a sub-unity superfluid fraction.

For brevity we will refer to the first approach as the density protocol and the second as the phase protocol. Since both approaches involve the application of a periodic spatially modulated potential, it seems natural to expect that both approaches should be described within a single framework. Also, some immediate questions emerge, such as: Why does the density protocol excite oscillations with two frequency components while the phase protocol excites only a single frequency? Superfluidity is inherently a long-wavelength property of the system, so how can it be determined by the phase protocol with a relatively short-wavelength excitation?

In this paper we develop a general linear response theory for probing supersolid states with one-dimensional crystal structure. This is most transparently developed for the translationally invariant case, which can be realized in experiments with a dipolar Bose-Einstein condensate (BEC) supersolid [3–5] confined in a ring geometry [see Fig. 1(a)]. This system and geometry has been the subject of several recent studies [1, 6, 7]. Neglecting curvature effects, the ring system is

equivalent to a finite interval of length L (corresponding to the ring circumference) and subject to periodic boundary conditions [Fig. 1(b)]. Previous work on the ground states and excitations of a purely linear geometry tube confined dipolar BEC [8–10] are in good qualitative agreement with calculations performed in the ring potential [1].

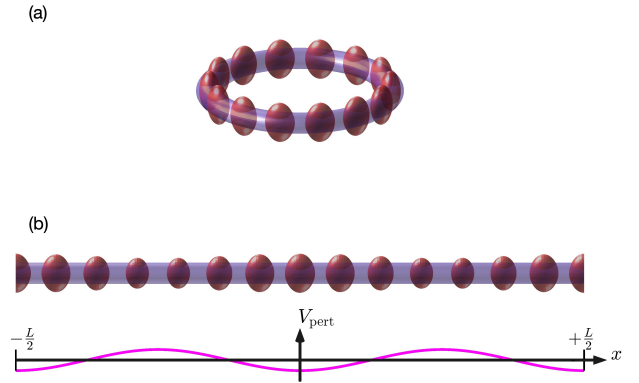


FIG. 1. Schematic image of system and perturbation. (a) A supersolid (red) in a ring-shaped trap (blue). (b) Equivalent (unwrapped) finite tube system of length L . Applied perturbation potential V_{pert} shown for reference.

In this work we will mainly illustrate our results using a soft-core model of a supersolid. This is purely a 1D supersolid model, with the advantage that the calculations are relatively straightforward compared to the dipolar tube model, which involves full 3D calculations and some intricate technical details of dealing with the singular dipole-dipole interactions. However, for probing along the supersolid [i.e. along the x -axis in Fig. 1(b)], and at sufficiently low energies that transverse excited states can be ignored, the 1D soft-core and tube dipolar systems behave similarly (e.g. see the comparisons made in Ref. [11]). Notably, both models have a continuous superfluid to supersolid phase transition, and exhibit two gapless excitation branches.

The outline of this paper is as follows. In Sec. II we introduce the density and phase protocols along with a brief description of the soft-core model. The system dynamics ob-

tained by solving the Gross-Pitaevskii (GP) equation are investigated, and the case of probing at the band-edge is discussed. We also propose generalized density and phase protocols, which removes the assumption that the perturbation and observable we probe are aligned to the supersolid. In Sec. III we present the linear response theory for the density and phase protocols, and the generalized protocols. We use this to understand the dynamics seen in Sec. II. In Sec. IV we present results for a supersolid with confinement along the x -axis to assess its effect on system behavior compared to the translationally invariant case. We focus on the question of superfluidity in Sec. V, discussing the relationship to hydrodynamic quantities and a Josephson-Junction array model. This allows us to make some comments on the suitability of the two protocols for determining superfluidity. Finally, we summarise and give concluding remarks in Sec. VI.

II. SPECTROSCOPY PROTOCOLS

A. System and perturbation

Consider a dilute BEC in a supersolid state confined in a ring geometry [Fig. 1(a), also see [1, 6, 7]]. We take the supersolid to have M_s lattice sites, and restrict our focus to the case where M_s is even¹. Both spectroscopy protocols we examine involve the application of the perturbation potential to the supersolid of the form $V_{\text{pert}} = -V_0 \cos(M\phi)$, where V_0 is the amplitude of the potential, ϕ is the azimuthal angle around the ring and M is a positive integer. For large ring diameters we can neglect curvature effects and map the system to a tube of length L , corresponding to the ring circumference [see Fig. 1(b)], and impose periodic boundary conditions on the tube. Here we introduce the x -axis as going around the tube axis with domain $-\frac{1}{2}L < x \leq \frac{1}{2}L$. The wavevector $k = 2\pi M/L$ describes the perturbation periodicity, i.e. $V_{\text{pert}} = -V_0 \cos(kx)$.

For a supersolid with lattice constant a , we will be interested in perturbation wavevectors k in the range $2\pi/L \leq k \leq Q$, where $Q \equiv \pi/a$ is the band-edge wavevector (i.e. half the reciprocal lattice vector). The lower limit being a single variation around the ring, which takes the limit $k \rightarrow 0$ for large L , accessing the long-wavelength excitations of the system. The upper limit corresponds to a periodic variation occurring over two sites. We avoid k being 0 or an integer multiple of the reciprocal lattice vector, as this would couple to zero energy excitations and linear response theory does not apply. The theory we develop here is more generally applicable to $k > Q$, but for wavevectors in our specified range, the perturbation most strongly couples to the lowest two gapless excitation bands, which are most sensitive to the many-body physics of the supersolid (cf. higher energy Bragg spectroscopy in Refs. [12, 13]).

To demonstrate the spectroscopy protocols and develop a linear response theory, we consider a straightforward supersolid model: a purely one-dimensional soft-core BEC. Because the low energy excitations of a 1D supersolid are universal in character, i.e. two gapless bands, and weak perturbations do not couple to the transverse excitations in a tube confined dipolar supersolid, the 1D soft-core system provides an appropriate platform for developing our theory with the general result being immediately applicable to the tube-dipolar case. For reference we note the comparison of a 3D tube dipolar supersolid to a 1D soft-core system in Ref. [11], which demonstrates the general similarities of these models.

We consider a BEC of N_T atoms on 1D domain of length L , with periodic boundary conditions. The atoms interact with a soft-core potential $U_{\text{sc}}(x) = U_0 \theta_H(a_{\text{sc}} - |x|)$, where θ_H is the Heaviside step function, a_{sc} is the core radius and U_0 is the potential strength. The meanfield description of this system is provided by the time-dependent GP equation $i\hbar\dot{\psi} = \mathcal{L}\psi$, where

$$\mathcal{L} = -\frac{\hbar^2}{2m} \frac{d^2}{dx^2} + V_{\text{pert}} + \int dx' U_{\text{sc}}(x-x') |\psi(x')|^2, \quad (1)$$

is the GP operator, and V_{pert} represents the applied perturbation. It is conventional to define the dimensionless interaction parameter

$$\Lambda = \frac{2ma_{\text{sc}}^3 U_0 N_T}{\hbar^2 L}. \quad (2)$$

A continuous transition occurs from a uniform to a modulated state at the critical value $\Lambda_c = 21.05$. Details about the excitations of this model are given in Sec. III A (also see Refs. [2, 14, 15]).

In solving for the supersolid ground states we choose for there to be a density peak (i.e. lattice site) at $x = 0$. This imposes an alignment with the potential [recall $V_{\text{pert}} = -V_0 \cos(kx)$] in that it has a trough at $x = 0$ [like the situation in Fig. 1(b), also see example ground state in Fig. 4(b)]. This alignment is explicit and necessary in the scheme of Ref. [2]. We revisit this assumption in Sec. II D where we introduce the generalized protocols and allow the perturbation (and observables) to be offset relative to the supersolid.

B. Density protocol

We first describe the Šindik *et al.* [1] proposal. Here the perturbation is considered to have been on for a long time such that the supersolid is in the ground state of the static perturbation. The perturbation strength is then suddenly set to zero at time $t = 0$, and the dynamics is examined. For this protocol the perturbation potential [i.e. perturbation appearing in Eq. (1)] has the form

$$V_{\text{pert}} \rightarrow V_d(x, t) = -V_0 \theta_H(-t) \cos(kx). \quad (3)$$

At $t > 0$ the translational invariance around the ring is restored by the sudden removal of the potential, however this causes longitudinal phonon modes to propagate through the

¹ This restriction is necessary to examine the proposal of Ref. [2], where an alternating phase is written on adjacent lattice sites.

supersolid. To quantify the excitation Šindik *et al.* [1] proposed measuring the linear density weighted by a cosine at wavevector k , i.e., the observable

$$F(t) = \int dx \cos(kx) |\psi(x, t)|^2, \quad (4)$$

and considered the evolution of $\delta F(t) \equiv F(t) - F_0$, where F_0 is the observable evaluated with the unperturbed supersolid ground state².

In Figs. 2(a) and (b) we show the dynamics of a soft-core supersolid state following the density protocol outlined above. In Fig. 2(a) we compare the dynamics of $\delta F(t)$ obtained from a GP simulation³ for various values of probe strength V_0 . These results show that for sufficiently small perturbation strengths ($V_0 \lesssim \hbar\omega_0$) the scaled observable $\delta F(t)/V_0$ is independent of V_0 , indicating that the system is in the linear response regime. Here we will focus on describing the behavior in the linear response regime, which we will later relate to system properties via linear response theory. When the system is probed with wave vector $k = Q/4$, $\delta F(t)$ clearly oscillates with two frequencies [i.e. Fig. 2(a)]. Similar results are obtained for any $k < Q$. This was the generic type of behavior explored in Ref. [1], who proposed fitting the response to two cosines to extract the properties of the two lowest excitation branches of the supersolid. In contrast, in Fig. 2(b), where the probe is at the band edge value $k = Q$, the response signal has a single dominant frequency.

C. Phase protocol

In Biagioni *et al.* [2] an alternative spectroscopy approach was suggested involving the application of a perturbation as a short and strong pulse to the supersolid ground state to imprint a phase profile. While this protocol was presented for the case $k = Q$, here we generalize it to any wavevector k . Taking the idealization of a delta-function pulse, the perturbation potential is

$$V_{\text{pert}} \rightarrow V_p(x, t) = -V_0 \delta t \delta(t) \cos(kx), \quad (5)$$

with dimensionless pulse area $V_0 \delta t / \hbar$. Immediately following the pulse ($t \rightarrow 0^+$) the wavefunction corresponds to the ground state of the unperturbed system, ψ_0 , with a phase written on it, i.e.

$$\psi(x, t = 0^+) = \psi_0(x) e^{iV_0 \delta t \cos(kx) / \hbar}. \quad (6)$$

Biagioni *et al.* considered the population and phase difference between adjacent sites as the relevant observables [see Sec. VB]. When there are strong connections between supersolid sites (i.e. when the supersolid does not consist of well-isolated droplets), defining the site population and phase is

somewhat arbitrary. Here we instead consider the F observable (4), noting that for $k = Q$, F corresponds to a weighted population difference of adjacent sites [i.e. the $\cos(Qx)$ factor positively (negatively) weights the population at even (odd) sites in this observable].

In Figs. 2(c) and (d) we show results for $\delta F(t)$ obtained from GP simulations following the phase protocol. Similar to the observations for the density protocol case, we observe that probing with a low k value [Fig. 2(c)] excites a response with two dominant frequency components, whereas at $k = Q$ [Fig. 2(d)] the response has a single dominant frequency.

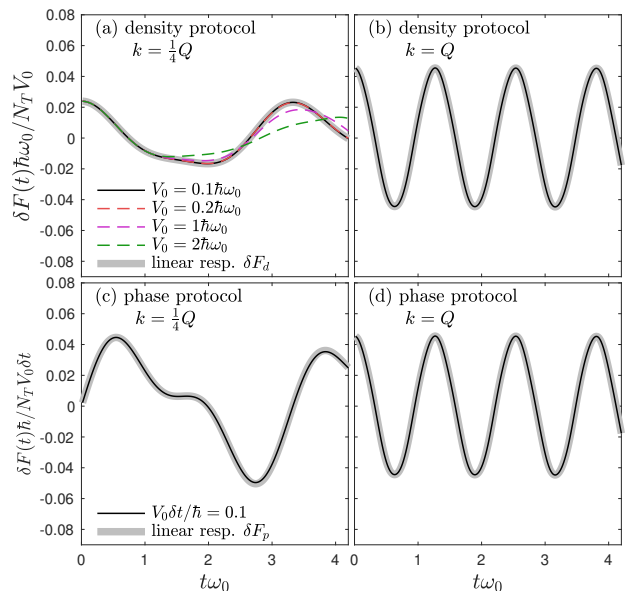


FIG. 2. Evolution of the observable $\delta F(t)$ following the spectroscopy protocols. (a), (b) Density protocol and (c), (d) phase protocol results. GP results (lines) and the linear response theory (thick grey line) are shown. In (a) the GP results are shown at various perturbation strengths to validate the linear response regime. In (b) $V_0 = 0.1\hbar\omega$, while in (c) and (d) $V_0 \delta t / \hbar = 0.1$. Ground state parameters: $\Lambda = 25$, $f_s = 0.705$ [see Sec. V] and $\mu = 24.2\hbar\omega_0$, where $\omega_0 = \hbar / ma_{\text{sc}}^2$. System length $L = 12.2a_{\text{sc}}$, supporting an $M_s = 8$ site supersolid.

D. General density and phase protocol

The previously introduced protocols have the perturbation and observable aligned to the supersolid (see discussion at the end of Sec. II A). This choice is most significant for $k = Q$ where the perturbation potential peaks and troughs all occur at the density peaks of the supersolid.

This motivates us to generalize the protocols to examine the effect of offsets of the perturbation and observable, relative to the supersolid. We can generalise the perturbation potential for the phase protocol to

$$V_p(x, t) = -V_0 \delta t \delta(t) \cos(kx - \varphi), \quad (7)$$

where φ is the phase offset of the perturbation, relative to the supersolid. Such an adjustment for the density protocol is

² Unless k is equal to a reciprocal lattice vector $F_0 = 0$.

³ Initial condition ($t = 0$) is the ground state with the static perturbation.

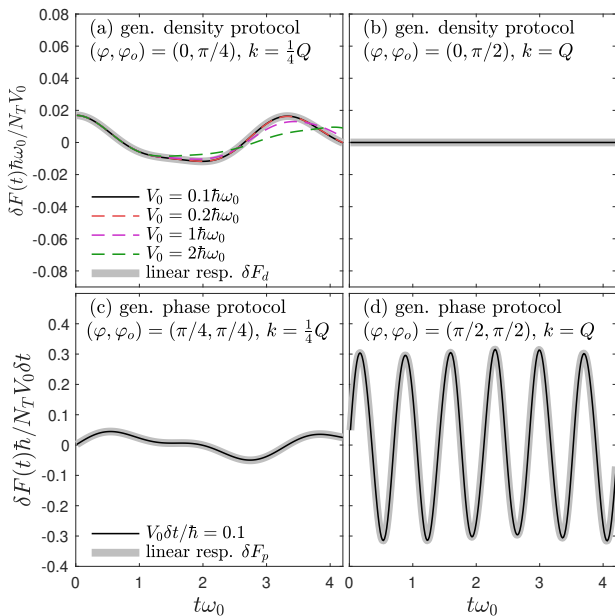


FIG. 3. Evolution of the observable $\delta F(t)$ following the generalized spectroscopy protocols. (a), (b) Generalized density protocol and (c), (d) generalized phase protocol results. GP results (lines) and the linear response theory (thick grey line) are shown. In (a) the GP results are shown at various perturbation strengths to validate the linear response regime. Other parameters as in Fig. 2.

redundant, because the supersolid ground state translates so that a lattice site (density peak) aligns with a potential minima (i.e. effectively returning to the $\varphi = 0$ case of V_d). However, for both protocols we can choose an arbitrary phase relative to the supersolid (φ_o) for the observable, i.e.

$$F(t) = \int dx \cos(kx - \varphi_o) |\psi(x, t)|^2. \quad (8)$$

Some results for the general spectroscopy protocols are shown in Fig. 3. The general density protocol results in Figs. 3(a) and (b) only differ from those in Figs. 2(a) and (b) by the observable phase φ_o . In these results $\delta F(t)$ is suppressed by a factor of $\cos \varphi_o$ relative to the respective earlier $\varphi_o = 0$ results. Notably, for Fig. 3(b), while the system is excited by the perturbation (i.e., same dynamics shown in Fig. 2(b)), the $\pi/2$ -displaced observable is insensitive to these dynamics, yielding $\delta F(t) = 0$.

The general phase protocol results in Figs. 3(c) and (d) can differ in both phases. For $\varphi = \varphi_o$ and $k < Q$, the response obtained from the general phase protocol is identical to the original phase protocol [cf. Figs. 2(c) and 3(c)]. For $k = Q$ we find that the response is sensitive to the phase choice. The case in Fig. 3(d) has a single frequency response, however, compared to Fig. 2(d), the response is much stronger and at a higher frequency. For $k = Q$ and $\varphi \neq \varphi_o$ (not shown) the response has two frequency components, being a combination of the results in Figs. 2(d) and 3(d).

III. LINEAR RESPONSE THEORY

Here we outline a linear response theory to describe the results obtained in the previous section, with additional details of the theory given in the Appendix. We begin by introducing the system excitations before presenting the linear response theory. Then we examine the nature of the excitations and the relevant dynamic structure factors to explain the general properties.

A. Excitations

The unperturbed ($V_{\text{pert}} = 0$) system ground state ψ_0 satisfies the time-independent GP equation $\mathcal{L}\psi_0 = \mu\psi_0$, where μ is the chemical potential and we take ψ_0 to be real. Note that $\int dx \psi_0^2 = N_T$. For supersolid ground states (with $\Lambda > \Lambda_c$) the excitations have a Bloch wave form and can be labelled by quasimomentum q in the first Brillouin zone, $q \in (-Q, Q]$, and band index ν . The excitation modes $\{u_{\nu q}(x), v_{\nu q}(x)\}$ and respective energies $\{\hbar\omega_{\nu q}\}$, satisfy the Bogoliubov-de Gennes (BdG) equations

$$\begin{bmatrix} \mathcal{L} + X - \mu & -X \\ X & -(\mathcal{L} + X - \mu) \end{bmatrix} \begin{bmatrix} u_{\nu q} \\ v_{\nu q} \end{bmatrix} = \hbar\omega_{\nu q} \begin{bmatrix} u_{\nu q} \\ v_{\nu q} \end{bmatrix}, \quad (9)$$

where X is defined so that

$$Xf = \psi_0(x) \int dx' U_{\text{sc}}(x - x') f(x') \psi_0(x'). \quad (10)$$

We show results for the spectrum of a translationally invariant supersolid in Fig. 4(a). From the boundary conditions the excitation quasimomenta are restricted to a discrete set determined by domain length L and the number of supersolid sites⁴. Continuous bands for the infinite system are shown for reference, and help reveal the two gapless excitation bands where the energy of the excitations vanishes as $q \rightarrow 0$. Labelling excitations by quasimomentum means that they are eigenstates of the translation operator. Because we have taken the supersolid to have a site at the origin, the system is also symmetric under the parity transformation. The intermediate states with $0 < |q| < Q$ occur as degenerate pairs with $\pm q$ in each band and relate to each other by the parity operator. Exceptions are the state $q = 0$ and $q = Q$, which are unique in each band and are eigenstates of the parity operator. As a result the quasiparticles at Q can be taken to be real and even or odd. We are not generally interested in $q = 0$ excitations, although this case describes ψ_0 , which can be taken to be a real even solution.

It is useful to consider the density fluctuation associated with a quasiparticle. This can be defined by adding a quasiparticle to the condensate, i.e. $\psi = \psi_0 + u_{\nu q} e^{-i\omega_{\nu q} t} - v_{\nu q}^* e^{i\omega_{\nu q} t}$. To leading order (since the quasi particle amplitudes are a factor of $\sim \sqrt{N_T}$ smaller than the condensate wavefunction) the

⁴ Allowed values are $q_n = \frac{2\pi n}{L}$, with $n \in \{-\frac{1}{2}M_s + 1, \dots, \frac{1}{2}M_s\}$ (cf. allowed perturbation wavevectors described in Sec. II A).

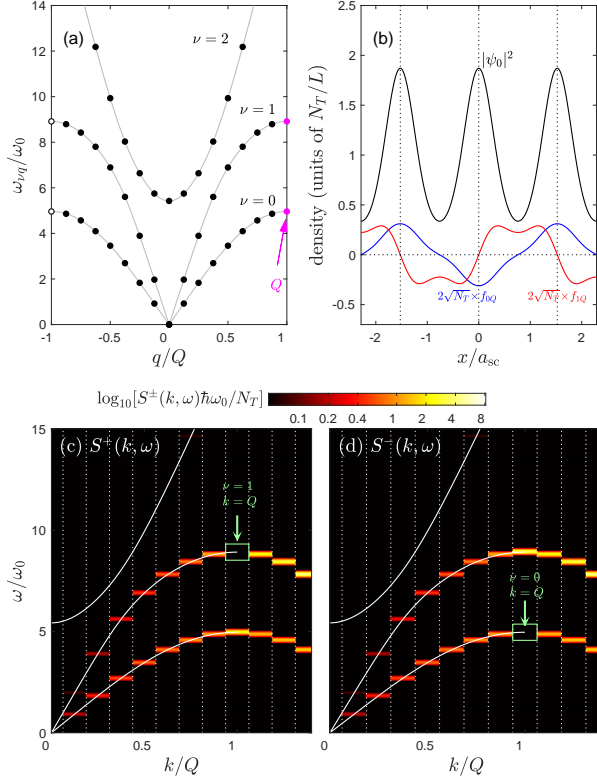


FIG. 4. Excitations and dynamic structure factors for the translationally invariant ring supersolid. (a) Excitation spectrum for a $M_s = 16$ site supersolid (filled markers) and the infinite system limit (lines). The edge-modes with quasimomentum Q are indicated. (b) Condensate density and the density fluctuations associated with the $\nu = 0$ and 1 edge-modes. The (c) S^+ and (d) S^- the dynamic structure factors with the delta functions broadened to $\delta(\omega) \rightarrow e^{-(\omega/\omega_B)^2}/\sqrt{\pi}\omega_B$, with $\omega_B = 0.1\omega_0$. Boxes and arrows indicate the edge state contribution to the dynamic structure factors. Other parameters as in Fig. 2.

spatial density fluctuation is $|\psi|^2 - \psi_0^2 \approx 2\text{Re}\{f_{\nu q}(x)e^{i\omega_{\nu q}t}\}$ where

$$f_{\nu q}(x) = [u_{\nu q}^*(x) - v_{\nu q}^*(x)]\psi_0(x). \quad (11)$$

In general the $f_{\nu q}(x)$ are complex functions, however for the edge states $q = Q$ they are real and of definite parity (inherited from the symmetry of ψ_0 and $\{u_{\nu Q}, v_{\nu Q}\}$ described above). We show $f_{\nu Q}(x)$ for the lowest two bands in Fig. 4(b). This reveals that the lowest band edge mode $\{\nu = 0, q = Q\}$ has a density fluctuation $f_{0Q}(x)$ causing population exchange (i.e. particle tunnelling) between adjacent sites. In contrast the first excited edge mode $f_{1Q}(x)$ causes the lattice sites to displace, with adjacent sites displacing in opposite directions.

B. General linear response theory

Linear response theory is well-established for a density coupled probe (e.g. see [16]). A summary of this theory, specialized to the general potential considered here, is presented

in the Appendix. This resulting prediction for the observable evolution is

$$\delta F_d(t) = \frac{V_0}{2} \sum_{\nu} \chi_{\nu}(k) \cos(\omega_{\nu \bar{k}} t), \quad (12)$$

$$\delta F_p(t) = \frac{V_0 \delta t}{2} \sum_{\nu} \omega_{\nu \bar{k}} \chi_{\nu}(k) \sin(\omega_{\nu \bar{k}} t), \quad (13)$$

for the general density and phase protocols, respectively⁵. Here \bar{k} denotes k reduced to the first Brillouin zone by an integer number of reciprocal lattice vectors. We have introduced

$$\chi_{\nu}(k) \equiv \chi_{\nu}^+(k) \cos \varphi \cos \varphi_o + \chi_{\nu}^-(k) \sin \varphi \sin \varphi_o, \quad (14)$$

being the ν -band contribution to the generalized static response function, where

$$\chi_{\nu}^{\pm}(k) = \sum_q \frac{|\langle \nu, q | \delta \hat{\rho}_k^{\pm} \pm \delta \hat{\rho}_k | 0 \rangle|^2}{\hbar \omega_{\nu q}}, \quad (15)$$

are the two quadrature components of the density fluctuation operator, $\delta \hat{\rho}_k$ (see Appendix). Here $|0\rangle$ denotes the quasiparticle vacuum state (i.e. ground state) and $|\nu, q\rangle$ denotes a state with a single $\{\nu, q\}$ -quasiparticle excited. Only excitations with $q = \pm \bar{k}$ contribute to $\chi_{\nu}^{\pm}(k)$, and we can evaluate these matrix elements as

$$\chi_{\nu}^{\pm}(k) = \frac{2|\delta \rho_{k, \nu \bar{k}}|^2}{\hbar \omega_{\nu \bar{k}}} \begin{cases} 1, & 0 < |\bar{k}| < Q, \\ 1 \pm (-1)^{\nu}, & \bar{k} = Q, \end{cases} \quad (16)$$

where

$$\delta \rho_{k, \nu q} \equiv \int dx e^{ikx} f_{\nu q}(x). \quad (17)$$

In Figs. 2 and 3 the linear response results (12) and (13) are shown for comparison to the GP results. Note that $\varphi = \varphi_o = 0$ for the results in Fig. 2 so that $\chi_{\nu}(k) \rightarrow \chi_{\nu}^+(k)$. An interesting feature is the distinct behavior of the edge mode contribution to Eq. (16). Notably, χ_{ν}^+ (χ_{ν}^-) is zero for odd (even) bands at $\bar{k} = Q$. In general the strong response comes from the lowest two bands and thus to a good approximation $\chi_{\nu}^+(Q)$ is determined by the edge mode of the ground band, whereas $\chi_{\nu}^-(Q)$ is determined by the edge mode of the first excited band. This explains the single frequency response observed in Figs. 2(b), (d) and 3(d). We can also understand this result from the symmetry of the excitations. For example, $\chi_{\nu}^+(Q)$ describes the coupling of the even-symmetry condensate orbital via the even-symmetry potential $\cos(kx)$ to the ν -band excitation at $q = Q$. Since the $\nu = 1$ band edge excitation is odd, this matrix element vanishes.

⁵ These two results are related because the two perturbations used in these protocols are related as $V_p = -\delta t \frac{\partial}{\partial t} V_d$.

C. Dynamic structure factors

For the cases where the excitation and observable are described by the same operator it is convenient to define a dynamic structure factor (see [16]). Here we do this for the two quadrature cases of the density fluctuation operator, i.e. $\delta\hat{\rho}_k^\pm \pm \delta\hat{\rho}_k$:

$$S^\pm(k, \omega) = \sum_{\nu, q} |\langle \nu, q | \delta\hat{\rho}_k^\pm \pm \delta\hat{\rho}_k | 0 \rangle|^2 \delta(\hbar\omega - \hbar\omega_{\nu q}), \quad (18)$$

$$= \sum_{\nu} \hbar\omega_{\nu\bar{k}} \chi_{\nu}^\pm(k) \delta(\hbar\omega - \hbar\omega_{\nu\bar{k}}), \quad (19)$$

utilizing expression (15) for the matrix elements.

We show results for the $S^\pm(k, \omega)$ dynamic structure factors in Figs. 4(c) and (d). These results indicate the strength of coupling to the various bands for different perturbation wavevectors k . Notably, we see that the majority of the weight resides in the lowest two bands, such that it is a reasonable approximation to truncate the sum over ν in Eqs. (12) and (13) to $\nu = 0$ and 1. These results also reveal the selective coupling of the edge states. Notably the $\{\nu = 1, Q\}$ -excitation vanishes in $S^+(k, \omega)$ and the $\{\nu = 0, Q\}$ -excitation vanishes in $S^-(k, \omega)$.

D. Low k behavior

For $0 < |k| < Q$, from result (16), we have that

$$\chi_{\nu}^\pm(k) \rightarrow \chi_{\nu}^{\rho}(k) = \frac{2|\delta\rho_{k, \nu k}|^2}{\hbar\omega_{\nu k}}, \quad (20)$$

where $\chi_{\nu}^{\rho}(k)$ is the ν -band contribution to the usual static density response function. The Šindik *et al.* [1] probing scheme was proposed for the long wavelength limit (and for $\varphi = \varphi_o$), such that (12) reduces to their result

$$\delta F_d(t) = \frac{V_0}{2} \sum_{\nu=0,1} \chi_{\nu}^{\rho}(k) \cos(\omega_{\nu k} t), \quad 0 < |k| < Q, \quad (21)$$

relating directly to the density response function. Applying similar arguments to the general phase protocol with $\varphi = \varphi_o$, allows us to write the small k linear response in terms of the static density response function as

$$\delta F_p(t) = \frac{V_0 \delta t}{2} \sum_{\nu=0,1} \omega_{\nu k} \chi_{\nu}^{\rho}(k) \sin(\omega_{\nu k} t), \quad 0 < |k| < Q. \quad (22)$$

IV. EXTENSION TO TRAPPED CASES

It is of interest to explore the application of the spectroscopy protocols to trapped cases where translational invariance is broken. In this section we consider two types of

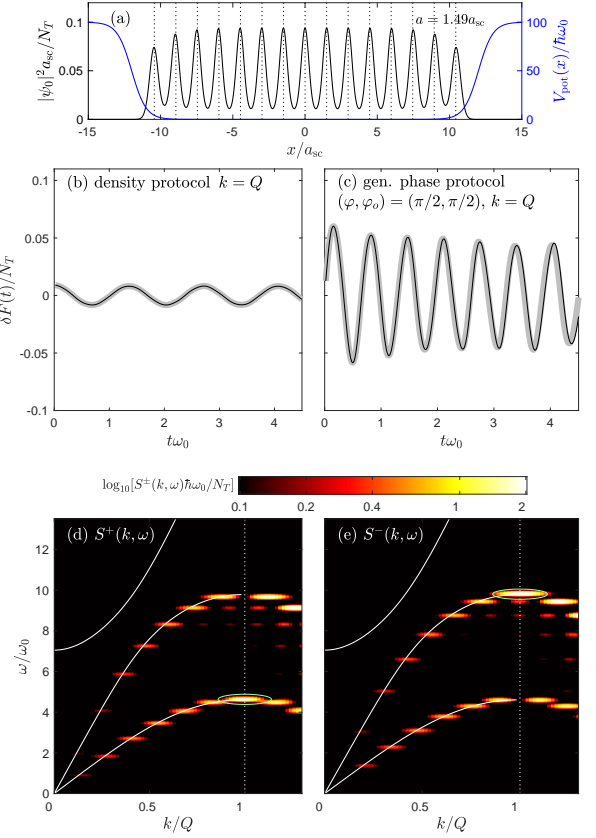


FIG. 5. Spectroscopy protocols applied to a box trapped super-solid. (a) Ground state density and trapping potential. Examples of (b) density and (c) generalized phase protocol responses for $V_0 = 0.2\hbar\omega_0$ and $V_0\delta t/\hbar = 0.2$, $\varphi = \varphi_o = \pi/2$, respectively. GP dynamics (black line) and linear response theory (thick grey line). (d) S^+ and (e) S^- the dynamic structure factors, frequency broadened as described in Fig. 4. Vertical dotted line indicates $k = Q$ and green ellipse indicates dominant feature at this wavevector. Excitation spectrum of translationally invariant case with $\Lambda = 27.3$ shown for comparison. (b,c) Black line is from GP simulation and grey thick line is the linear response result determined from the BdG excitations. Results for a box trap potential $V_{\text{pot}} = 50\hbar\omega_0[\tanh(|x/a_{sc}| - 12) + 1]$, with $N_T U_0 = 300\hbar\omega_0$.

trapped systems that could be explored in experiments: a box-shaped trap and a harmonic trap. The results for these two systems are presented in Figs. 5 and 6. In both cases subplot (a) shows the ground state density and the trapping potential for reference. The lattice sites are not strictly equally spaced in the presence of an external potential, but in both cases the peak spacing is well characterized by an average lattice constant a (with corresponding lattice sites indicated by vertical dotted lines). We use a to define the reciprocal lattice vector for the spectroscopy protocols. Here we choose to focus on band edge probing, i.e., Eqs. (3) and (5) with $k = Q$.

Results of the GP simulations of the dynamics are shown in subplots (b) and (c). This is seen to be in good agreement with the linear response theory. Because these systems are not translationally invariant, ν and q are not good quantum

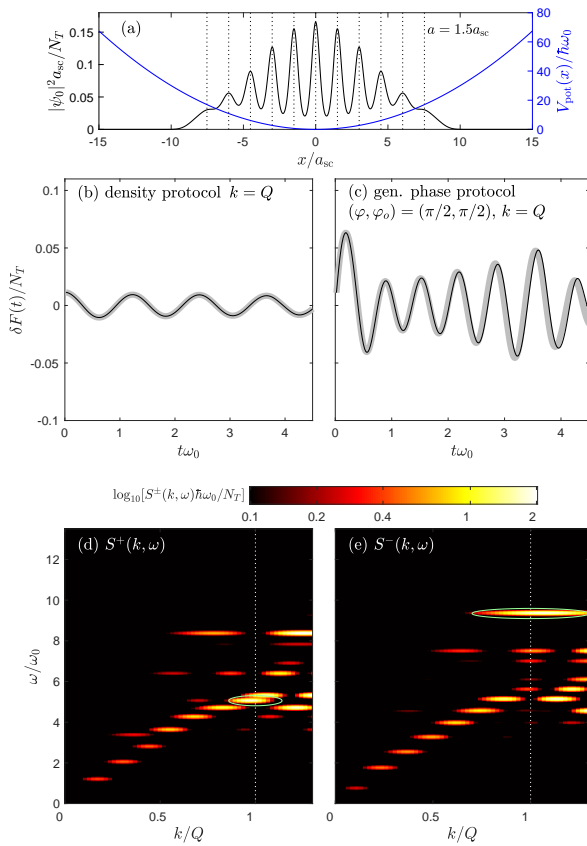


FIG. 6. Spectroscopy protocols applied to a harmonically trapped supersolid. (a) Ground state density and trapping potential. Examples of (b) density and (c) generalized phase protocol responses for $V_0 = 0.2\hbar\omega_0$ and $V_0\delta t/\hbar = 0.2$, $\varphi = \varphi_0 = \pi/2$, respectively. (d) S^+ and (e) S^- the dynamic structure factors, frequency broadened as described in Fig. 4. Vertical dotted line indicates $k = Q$ and green ellipse indicates dominant feature at this wavevector. (c,d) Black line is from GP simulation and grey thick line is the linear response result determined from BdG calculations. Inset to (c) shows the ground state density profile. Results for the harmonic trap $V_{\text{pot}} = 0.3(x/a_{\text{sc}})^2\hbar\omega_0$, with $N_T U_0 = 175\hbar\omega_0$.

numbers, and the response is determined by summing over all excitation modes [see Eqs. (43) to (46), which generalize the linear response theory of Eqs. (12), (13) and (16)].

The box-trapped case has a relatively uniform average density [see Fig. 5(a)] and the dynamic structure factors reveal a clear band structure comparable to the translationally invariant results [cf. Figs. 5(d) and (e) and Figs. 4(c) and (d)]. To make a more direct comparison we can map the parameters to a similar translationally invariant case: the length of the box trapped state is $L \approx 22a_{\text{sc}}$, giving a dimensionless interaction parameter $\Lambda \approx 27.3$ [from Eq. (2)]. The corresponding excitation bands for the infinite translationally invariant system at this value of Λ are shown in Figs. 5(d) and (e) and seen to be in good quantitative agreement with the dynamic structure factor. We see the selective edge-mode behavior in these results. Notably, a mode of the lowest band at $k \approx Q$ is seen to contribute strongly to S^+ but is absent from S^- [indicated

by ellipse in Fig. 5(d)], and a mode of the first excited band at $k \approx Q$ is seen to contribute strongly to S^- but is absent from S^+ [indicated by ellipse in Fig. 5(e)].

In the harmonically trapped system the average density varies across the sample, although there is still a reasonably well-defined average lattice constant [see Fig. 6(a)]. Here the response function does not reveal two clearly defined low energy bands like in the box-trapped case [Fig. 6(d) and (e)]. Although at the band-edge we again see a strong contribution from a low energy mode to S^+ that is absent from S^- [indicated by ellipse in Fig. 6(d)] and a strong contribution from a higher energy mode to S^- that is absent from S^+ [indicated by ellipse in Fig. 6(e)]. However, the presence of other weaker modes with weight at the band edge is less clear, particularly for the case sensitive to probing an observable related to S^- [i.e. Fig. 6(c)] where a beating between several frequencies is apparent.

V. RELATIONSHIP TO SUPERFLUIDITY

The spectroscopy proposal by Šindik *et al.* [1] and the spectroscopy experiment by Biagioni *et al.* [2] were applied to determine the superfluid fraction. This is of interest because the superfluid fraction of a supersolid at zero temperature is reduced from unity, even when the condensate fraction is unity. In general the superfluid fraction is determined by examining the response (current or energy) of the system to a small imposed phase gradient (i.e., imposed phase twist $\Delta\theta$ over the length of the system or equivalently a superfluid velocity $v_s = \hbar\Delta\theta/mL$) [8, 17–19]. For example, by analysing the energy response, we have that the superfluid fraction is

$$f_s = \frac{1}{mN_T} \frac{\partial^2 E}{\partial v_s^2}, \quad (23)$$

where E is the energy functional. Leggett developed an upper bound for the superfluid fraction in terms of the system density profile [17, 20]

$$f_s^+ = \frac{L}{\rho} \left(\int dx \frac{1}{|\psi_0(x)|^2} \right)^{-1}, \quad (24)$$

where $\rho = N_T/L$ is the average density. This bound is exact for the 1D soft-core model, and is an accurate estimate for 1D dipolar supersolids (e.g. see results in Ref. [9]).

Recently two experiments determined the superfluid fraction of a BEC in an optical lattice [21, 22] validating the Leggett bound. In this case the superfluid fraction is related to the speed of sound (in the optical lattice) c as

$$f_s = \frac{c^2}{c_\kappa^2}, \quad (25)$$

where $m c_\kappa^2 \equiv (\rho\kappa)^{-1}$, with κ being the compressibility. For a supersolid, the spontaneously broken translational symmetry leads to the emergence of another gapless excitation band. A 1D supersolid exhibits two speeds of sound [8, 10, 11, 23, 24] and the simple result (25) no longer holds.

A. Supersolid hydrodynamics: Long wavelength spectroscopy

The hydrodynamic theory for Galilean invariant supersolids (e.g. see [11, 25–30]) furnishes a relationship between the superfluid fraction and the speeds of sound for a supersolid:

$$f_s = \frac{c_1^2 c_0^2}{c_\kappa^2 (c_1^2 + c_0^2 - c_\kappa^2)}. \quad (26)$$

Here c_0 and c_1 are the speeds of sound of the lowest two (longitudinal) gapless excitation bands.

Šindik *et al.* [1] showed that performing density spectroscopy for $|k| \ll Q$ can determine the quantities in this expression for f_s . Notably, measuring the response and fitting the results to Eq. (21) determines $\omega_{\nu k}$ and $\chi_\nu^\rho(k)$ for $\nu = 0, 1$ [cf. Fig. 2(a) as an example of spectroscopy in this regime]. This information gives the speeds of sound for the lowest two branches, i.e. $c_\nu = \lim_{k \rightarrow 0} \omega_{\nu k}^\rho / k$ and the compressibility $\kappa = \rho^{-1} \lim_{k \rightarrow 0} \sum_\nu \chi_\nu^\rho(k)$.

This approach applies to the translationally invariant supersolid, and was specifically formulated for a dipolar supersolid in a ring trap. It has the disadvantage that the time scales of low- k modes are slow, thus requiring long observation times to make the required fits. Furthermore, the density protocol requires a long initialisation step, i.e., waiting sufficiently long for the system to relax to the ground state of the perturbation before it is removed and the observable is measured. Long time scales pose a challenge for dipolar supersolid experiments, where three-body loss tends to limit the lifetime. For this reason the phase protocol might be favorable for experiments, because it provides access to the same quantities [i.e. by fitting the response to Eq. (22)], yet does not require the initialisation step.

B. Josephson-Junction array theory: Band-edge spectroscopy

A Josephson-Junction array (JJA) is a model for a BEC in an optical lattice [31, 32] (also see [33]) and is an appealing model for a supersolid, where it can describe the coherent atom tunnelling dynamics between sites [34] (also see [35]). This model involves two parameters, the tunnel coupling between sites J and the interaction parameter U , describing the interactions at each site. The system is then specified by the number of atoms N_j at site j and the phase of these atoms θ_j [see Fig. 7(a)]. Within the JJA model the superfluid fraction is given by [from Eq. (23)]

$$f_s = \frac{J m a^2}{\hbar^2}, \quad (27)$$

and thus can be determined by measuring J .

Here we analyse the appropriateness of the JJA model for a translationally invariant supersolid where the ground state has $\bar{N} = N_T / M_s$ atoms at each site. We focus on the band-edge excitation of the system, where the disturbance alternates at adjacent sites, schematically shown as a density wave in Fig. 7(a). Following [2] we refer to the periodic

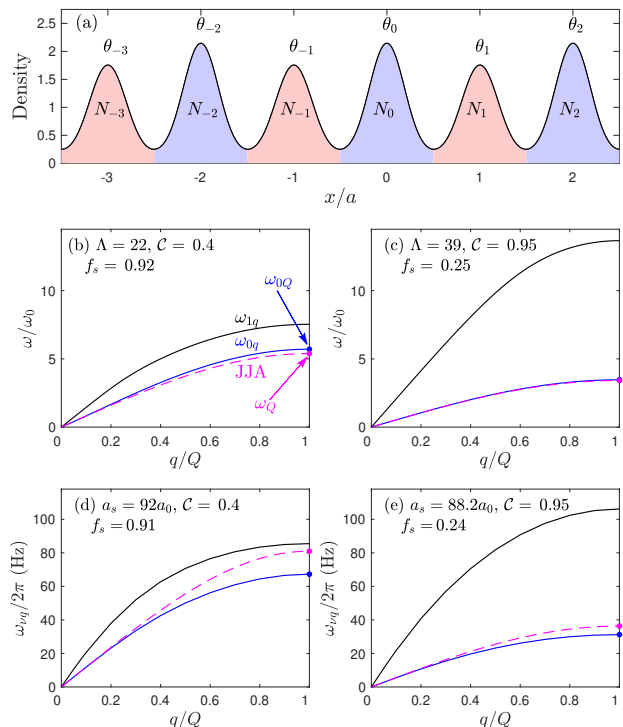


FIG. 7. (a) Schematic of JJA model of a supersolid indicating the number N_j and phase θ_j at site j . Here showing the case of an instantaneous population imbalance between even and odd sites, characteristic of the (band-edge) Josephson oscillation mid-cycle. Comparison of the JJA mode excitations (dashed magenta line) and BdG calculations for the lowest sound excitation bands (blue and black lines) for (b), (c) the 1D soft-core and (d), (e) tube dipolar supersolid states. Parameters indicated in subplots. The dipolar results are from the data set used in Refs. [19] to describe a ^{164}Dy condensate of linear density $\rho = 2500 \mu\text{m}^{-1}$ with radial confinement of 150 Hz.

oscillation dynamics of this state as being Josephson oscillation (cf. DC Josephson effect for supersolids discussed in Ref. [36]). Note, this is the kind of state and the dynamics occurring in Figs. 2(b) and (d). In this case all even sites are equivalent and all odd sites are equivalent, and we can study the dynamics in terms of the variables $\Delta N = N_1 - N_0$ and $\Delta\theta = \theta_1 - \theta_0$, being the atom number difference and phase difference between adjacent sites. For a weak perturbation from equilibrium (i.e., cases where $|\Delta N| \ll \bar{N}$ and $|\Delta\theta| \ll 1$) the dynamics of these quantities satisfies the Josephson-like equations [37]

$$\hbar \Delta \dot{N} = 8 \bar{N} J \Delta \theta, \quad (28)$$

$$\hbar \Delta \dot{\theta} = -\frac{1}{\bar{N}} (2J + \bar{N}U) \Delta N, \quad (29)$$

with a harmonic solution of frequency

$$\omega_Q = \hbar^{-1} \sqrt{4J(4J + 2\bar{N}U)}. \quad (30)$$

Biagioni *et al.* [2] used the phase protocol at $k = Q$ to write a phase difference on adjacent sites of the supersolid, thus exciting the Josephson oscillation [cf. Fig. 2(d) as an example of

spectroscopy in this regime]. Measuring this frequency (ω_Q) in the experiment, and with the additional input of U from calculations, determines the value of J [from Eq. (30)], and hence the superfluid fraction f_s via Eq. (27).

As noted in Refs. [34, 35], the neglect of the crystal motion in the JJA, means this model is incomplete. Here we test its applicability by making a direct comparison of the JJA model to two supersolids: the 1D soft-core system we have discussed thus far in the paper, and a 1D dipolar supersolid (the physical system studied in Ref. [2]). We compare the excitations of the JJA model to those for the supersolid system obtained by numerical calculations of the BdG equations. The results for the dipolar system are from the data presented in Ref. [10] and we refer to that paper for the theoretical description of the system and calculation details. While the JJA has a single gapless band the supersolids have two gapless bands [see Figs. 7(b)-(e)]. The lowest band of these bands, known as second sound or the phase band, is the relevant band for comparison to the JJA result. This band is dominated by the tunnelling of atoms between sites, analogous to the physics described by the JJA. The upper band of the supersolid, known as first sound or the density band, is predominantly a crystal phonon-like excitation, i.e., involves a deformation of the supersolid crystal lattice.

The excitations of the translationally invariant JJA has the analytic form [38]

$$\omega_q = \sqrt{\omega_q^0(\omega_q^0 + 2\bar{N}U/\hbar)}, \quad (31)$$

where $\hbar\omega_q^0 = 4J \sin^2(qa/2)$ and q is the quasimomentum. To make the comparison it is necessary to determine the parameters U and J . In deep optical lattices where this can be done using localized Wannier orbitals [33, 39, 40], however this approach is inapplicable to supersolids where there is significant overlap between sites. Here we identify U and J to reproduce the long-wavelength hydrodynamic properties of the supersolids. The two hydrodynamic properties we use are the superfluid fraction f_s and the speed of sound of the lowest band c_0 . These quantities are both determined from the numerical calculations of the BdG equations [Eq. (9) and Ref. [10]] and ground state properties [Eq. (23) and Refs. [9, 19]]. From f_s and c_0 the values of J and U in the corresponding JJA are thus determined: f_s gives J using Eq. (27), and subsequently c_0 fixes the value of U using the relationship

$$c_0 = \frac{a}{\hbar} \sqrt{2J\bar{N}U}, \quad (32)$$

[from Eq. (31)].

Figure 7 presents comparisons for two cases of each for each supersolid system: (b,d) a relatively low contrast (high superfluid fraction) state and (c,e) a high contrast (low superfluid fraction) state. Here the contrast is defined as

$$\mathcal{C} = \frac{\rho_{\max} - \rho_{\min}}{\rho_{\max} + \rho_{\min}}, \quad (33)$$

where ρ_{\max} (ρ_{\min}) is the maximum (minimum) of the linear density, with $\mathcal{C} = 0$ being the uniform superfluid state,

and $\mathcal{C} = 1$ being where the linear density goes to zero between sites. The agreement between the JJA model dispersion relation ω_q and supersolid lowest band ω_{0q} is assured for $q \rightarrow 0$ because of our choice of parameters to match the hydrodynamic properties. The deviation for large q thus reveals physics beyond the JJA model in the supersolids. Most importantly for the Biagioni *et al.* [2] scheme is the comparison of the frequency or band-edge mode, i.e., the Josephson oscillation frequency ω_Q , as this is the quantity that they measure experimentally. This mode is beyond the hydrodynamic description (due to its short wavelength), and its relationship to the hydrodynamic properties, and particularly the superfluid fraction, relies on the appropriateness of the JJA model. We have indicated the edge modes for comparison in Figs. 7(b)-(e). Notably, the relevant ω_{0Q} mode from the supersolid excitations. In general we find that agreement between ω_Q and ω_{0Q} is quite reasonable for the cases we have examined, although it is noticeably better for the soft-core supersolid. We understand this as arising because the soft-core model tends to have a more rigid lattice than the dipolar supersolid, as revealed by studies of the elastic properties of these supersolids [11]. For the dipolar supersolid case of Fig. 7(d) the relative difference between ω_Q and ω_{0Q} is about 20%, and this would be reflected in an error in the inferred value of f_s .

VI. CONCLUSION

In this work, we introduced a linear response description linking and generalizing the density and phase protocols presented separately in recent works. We illustrate the theory using a soft-core model of a supersolid, but the theory is more generally applicable. For a translationally invariant system both protocols tend to excite excitations from two lowest gapless excitation bands with a wavevector set by the perturbation. Interestingly, our theory explains the peculiar behavior observed at the band edge—where only a single excitation responds at a wavelength twice the lattice constant. This phenomenon arises due to the symmetry of the edge modes, which can be selectively excited depending on the alignment of the external potential with respect to the supersolid crystal, i.e., via the generalized probing scheme we suggest.

We present results for trapped cases, where the translational invariance is broken, finding the band-edge feature of excitations still approximately holds. Finally, we have discussed the superfluid fraction of a supersolid, and how this relates to hydrodynamic theory and a Josephson-Junction array model. These results provide valuable insights into the use of spectroscopy protocols for determining the superfluid fraction and deepen our understanding of supersolid excitations.

ACKNOWLEDGMENTS

The authors acknowledge M. Cui and W. Cresswell for early work exploring Josephson dynamics in a supersolid that informed this study and funding from the Marsden Fund of the Royal Society of New Zealand.

APPENDIX: LINEAR RESPONSE THEORY

Within the framework of Bogoliubov theory the field operator can be expressed as

$$\hat{\psi}(x) = \psi_0(x) + \sum_j [u_j(x)\hat{\alpha}_j - v_j^*(x)\hat{\alpha}_j^\dagger], \quad (34)$$

where $\{\hat{\alpha}_j, \hat{\alpha}_j^\dagger\}$ are bosonic mode operators which satisfy the commutation relations $[\hat{\alpha}_i, \hat{\alpha}_j^\dagger] = \delta_{ij}$. Here the excitations modes $\{u_j(x), v_j(x)\}$ (with respective energies $\{\hbar\omega_j\}$) are the generalization of Eq. (9) to allow for an external potential, such that quasimomentum is not a good quantum number, and we introduce the general index j .

The density fluctuation operator, $\delta\hat{\rho}_k^\dagger = \int dx e^{ikx}(\hat{\psi}^\dagger\hat{\psi} - \psi_0^2)$, to first order in the quasiparticle operators, is given by

$$\delta\hat{\rho}_k^\dagger = \sum_j (\delta\rho_{k,j}\hat{\alpha}_j^\dagger + \delta\rho_{-k,j}^*\hat{\alpha}_j), \quad (35)$$

where we have defined the matrix element as

$$\delta\rho_{k,j} \equiv \langle j|\delta\hat{\rho}_k^\dagger|0\rangle \quad (36)$$

$$= \int dx e^{ikx} [u_j(x) - v_j(x)]^* \psi_0(x), \quad (37)$$

with $|0\rangle$ being the quasiparticle vacuum state, and $|j\rangle = \hat{\alpha}_j^\dagger|0\rangle$ being a state with a single j -quasiparticle. The density fluctuation operator is useful because the perturbation potential can be written in second quantized form as

$$\hat{V} = -\frac{1}{2}V_0(t)(\delta\hat{\rho}_k^\dagger e^{-i\varphi} + \delta\hat{\rho}_k e^{i\varphi}), \quad (38)$$

where $V_0(t) = V_0\theta_H(-t)$ for the generalized density protocol or $V_0(t) = V_0\delta t\delta(t)$ for the phase protocol. Using time-dependent perturbation theory we obtain the following expressions for the response evolution

$$\delta F_d(t) = V_0 \sum_j \frac{1}{4\hbar\omega_j} [c_j(k)e^{-i\omega_j t} + c_j^*(k)e^{i\omega_j t}], \quad (39)$$

$$\delta F_p(t) = V_0\delta t \sum_j \frac{i}{4\hbar} [c_j(k)e^{-i\omega_j t} - c_j^*(k)e^{i\omega_j t}], \quad (40)$$

for the density and phase protocols, respectively, where

$$c_j(k) = \delta\rho_{-k,j}^*\delta\rho_{k,j}e^{-i(\varphi+\varphi_o)} + \delta\rho_{k,j}^*\delta\rho_{-k,j}e^{i(\varphi+\varphi_o)} + |\delta\rho_{k,j}|^2e^{-i(\varphi-\varphi_o)} + |\delta\rho_{-k,j}|^2e^{i(\varphi-\varphi_o)}. \quad (41)$$

For the trapped supersolid, $u_j - v_j$ can be taken to be real, so that $\delta\rho_{k,j} = \delta\rho_{-k,j}^*$, and either even ($\delta\rho_{k,j} = \delta\rho_{-k,j}$) giving $c_j(k) = 4|\delta\rho_{k,j}|^2 \cos\varphi \cos\varphi_o$ or odd ($\delta\rho_{k,j} = -\delta\rho_{-k,j}$)

giving $c_j(k) = 4|\delta\rho_{k,j}|^2 \sin\varphi \sin\varphi_o$, which can be written as

$$c_j(k) = |\delta\rho_{k,j} + \delta\rho_{-k,j}|^2 \cos\varphi \cos\varphi_o + |\delta\rho_{k,j} - \delta\rho_{-k,j}|^2 \sin\varphi \sin\varphi_o. \quad (42)$$

Thus the previous results can be written in the form

$$\delta F_d(t) = \frac{V_0}{2} \sum_j \chi_j(k) \cos(\omega_j t), \quad (43)$$

$$\delta F_p(t) = \frac{V_0\delta t}{2} \sum_j \omega_j \chi_j(k) \sin(\omega_j t), \quad (44)$$

with

$$\chi_j(k) \equiv \chi_j^+(k) \cos\varphi \cos\varphi_o + \chi_j^-(k) \sin\varphi \sin\varphi_o, \quad (45)$$

being the j -band contribution to the generalized static response function, where

$$\chi_j^\pm(k) = \frac{|\langle j|\delta\hat{\rho}_k^\dagger \pm \delta\hat{\rho}_k|0\rangle|^2}{\hbar\omega_j}. \quad (46)$$

For the translationally invariant supersolid the matrix elements become

$$\delta\rho_{k,j} \rightarrow \delta\rho_{k,\nu q} = \int dx e^{ikx} [u_{\nu q}^*(x) - v_{\nu q}^*(x)]\psi_0(x), \quad (47)$$

with the selection rule $k = q + 2nQ$, where n is an integer. Then, for $0 < |q| < Q$, $|\delta\rho_{-k,\nu-q}|^2 = |\delta\rho_{k,\nu q}|^2$ and $\delta\rho_{k,\nu q} \neq 0 \implies \delta\rho_{-k,\nu q} = 0$ so

$$c_{\nu q}(k) + c_{\nu-q}(k) = 2(|\delta\rho_{k,\nu q}|^2 + |\delta\rho_{-k,\nu q}|^2) \cos(\varphi - \varphi_o). \quad (48)$$

Also, $\delta\rho_{-k,\nu Q} = (-1)^\nu \delta\rho_{k,\nu Q}$, so

$$c_{\nu Q}(k) = 2|\delta\rho_{k,\nu Q}|^2 [\cos(\varphi - \varphi_o) + (-1)^\nu \cos(\varphi + \varphi_o)], \quad (49)$$

i.e.

$$\delta F_d(t) = \frac{V_0}{2} \sum_\nu \chi_\nu(k) \cos(\omega_{\nu\bar{k}} t), \quad (50)$$

$$\delta F_p(t) = \frac{V_0\delta t}{2} \sum_\nu \omega_{\nu\bar{k}} \chi_\nu(k) \sin(\omega_{\nu\bar{k}} t), \quad (51)$$

with

$$\chi_\nu(k) = \frac{2|\delta\rho_{k,\nu\bar{k}}|^2}{\hbar\omega_{\nu\bar{k}}} [\cos(\varphi - \varphi_o) + (-1)^\nu \cos(\varphi + \varphi_o)\delta_{\bar{k},Q}] \quad (52)$$

which gives (14) using

$$\chi_\nu^\pm(k) = \sum_q \frac{|\langle \nu, q|\delta\hat{\rho}_k^\dagger \pm \delta\hat{\rho}_k|0\rangle|^2}{\hbar\omega_{\nu q}} = \sum_q \frac{|\delta\rho_{k,\nu q} \pm \delta\rho_{-k,\nu q}|^2}{\hbar\omega_{\nu q}}. \quad (53)$$

- [1] M. Šindik, T. Zawislak, A. Recati, and S. Stringari, Sound, superfluidity, and layer compressibility in a ring dipolar supersolid, *Phys. Rev. Lett.* **132**, 146001 (2024).
- [2] G. Biagioni, N. Antolini, B. Donelli, L. Pezzè, A. Smerzi, M. Fattori, A. Fioretti, C. Gabbanini, M. Inguscio, L. Tanzi, and G. Modugno, Measurement of the superfluid fraction of a supersolid by Josephson effect, *Nature* **629**, 773 (2024).
- [3] L. Tanzi, E. Lucioni, F. Famà, J. Catani, A. Fioretti, C. Gabbanini, R. N. Bisset, L. Santos, and G. Modugno, Observation of a dipolar quantum gas with metastable supersolid properties, *Phys. Rev. Lett.* **122**, 130405 (2019).
- [4] F. Böttcher, J.-N. Schmidt, M. Wenzel, J. Hertkorn, M. Guo, T. Langen, and T. Pfau, Transient supersolid properties in an array of dipolar quantum droplets, *Phys. Rev. X* **9**, 011051 (2019).
- [5] G. Natale, R. M. W. van Bijnen, A. Patscheider, D. Petter, M. J. Mark, L. Chomaz, and F. Ferlaino, Excitation spectrum of a trapped dipolar supersolid and its experimental evidence, *Phys. Rev. Lett.* **123**, 050402 (2019).
- [6] M. Nilsson Tengstrand, P. Stürmer, J. Ribbing, and S. M. Reimann, Toroidal dipolar supersolid with a rotating weak link, *Phys. Rev. A* **107**, 063316 (2023).
- [7] J. Hertkorn, P. Stürmer, K. Mukherjee, K. S. H. Ng, P. Uerlings, F. Hellstern, L. Lavoine, S. M. Reimann, T. Pfau, and R. Klemt, Decoupled sound and amplitude modes in trapped dipolar supersolids, *Phys. Rev. Res.* **6**, L042056 (2024).
- [8] S. M. Roccuzzo and F. Ancilotto, Supersolid behavior of a dipolar Bose-Einstein condensate confined in a tube, *Phys. Rev. A* **99**, 041601 (2019).
- [9] J. C. Smith, D. Baillie, and P. B. Blakie, Supersolidity and crystallization of a dipolar Bose gas in an infinite tube, *Phys. Rev. A* **107**, 033301 (2023).
- [10] P. B. Blakie, L. Chomaz, D. Baillie, and F. Ferlaino, Compressibility and speeds of sound across the superfluid-to-supersolid phase transition of an elongated dipolar gas, *Phys. Rev. Res.* **5**, 033161 (2023).
- [11] L. M. Platt, D. Baillie, and P. B. Blakie, Sound waves and fluctuations in one-dimensional supersolids, *Phys. Rev. A* **110**, 023320 (2024).
- [12] D. Petter, A. Patscheider, G. Natale, M. J. Mark, M. A. Baranov, R. van Bijnen, S. M. Roccuzzo, A. Recati, B. Blakie, D. Baillie, L. Chomaz, and F. Ferlaino, Bragg scattering of an ultracold dipolar gas across the phase transition from Bose-Einstein condensate to supersolid in the free-particle regime, *Phys. Rev. A* **104**, L011302 (2021).
- [13] L. Chomaz, Probing the supersolid order via high-energy scattering: analytical relations among the response, density modulation, and superfluid fraction, *Phys. Rev. A* **102**, 023333 (2020).
- [14] M. Kunimi and Y. Kato, Mean-field and stability analyses of two-dimensional flowing soft-core bosons modeling a supersolid, *Phys. Rev. B* **86**, 060510 (2012).
- [15] S. Prestipino, A. Sergi, and E. Bruno, Freezing of soft-core bosons at zero temperature: A variational theory, *Phys. Rev. B* **98**, 104104 (2018).
- [16] L. Pitaevskii and S. Stringari, *Bose-Einstein Condensation and Superfluidity* (Oxford University Press, Oxford, 2016).
- [17] A. J. Leggett, Can a solid be "superfluid"?, *Phys. Rev. Lett.* **25**, 1543 (1970).
- [18] N. Sepúlveda, C. Josserand, and S. Rica, Superfluid density in a two-dimensional model of supersolid, *Euro. Phys. J. B* **78**, 439 (2010).
- [19] P. B. Blakie, Superfluid fraction tensor of a two-dimensional supersolid, *J. Phys. B* **57**, 115301 (2024).
- [20] N. Sepúlveda, C. Josserand, and S. Rica, Nonclassical rotational inertia fraction in a one-dimensional model of a supersolid, *Phys. Rev. B* **77**, 054513 (2008).
- [21] G. Chauveau, C. Maury, F. Rabec, C. Heintze, G. Brochier, S. Nascimbene, J. Dalibard, J. Beugnon, S. M. Roccuzzo, and S. Stringari, Superfluid fraction in an interacting spatially modulated Bose-Einstein condensate, *Phys. Rev. Lett.* **130**, 226003 (2023).
- [22] J. Tao, M. Zhao, and I. B. Spielman, Observation of anisotropic superfluid density in an artificial crystal, *Phys. Rev. Lett.* **131**, 163401 (2023).
- [23] H. Watanabe and T. Brauner, Spontaneous breaking of continuous translational invariance, *Phys. Rev. D* **85**, 085010 (2012).
- [24] T. Ilg and H. P. Büchler, Ground-state stability and excitation spectrum of a one-dimensional dipolar supersolid, *Phys. Rev. A* **107**, 013314 (2023).
- [25] A. F. Andreev and I. M. Lifshitz, Quantum theory of defects in crystals, *Sov. Phys. JETP* **29**, 1107 (1969).
- [26] W. M. Saslow, Microscopic and hydrodynamic theory of superfluidity in periodic solids, *Phys. Rev. B* **15**, 173 (1977).
- [27] D. T. Son, Effective Lagrangian and topological interactions in supersolids, *Phys. Rev. Lett.* **94**, 175301 (2005).
- [28] C. Josserand, Y. Pomeau, and S. Rica, Patterns and supersolids, *Eur. Phys. J.: Spec.* **146**, 47 (2007).
- [29] C.-D. Yoo and A. T. Dorsey, Hydrodynamic theory of supersolids: variational principle, effective Lagrangian, and density-density correlation function, *Phys. Rev. B* **81**, 134518 (2010).
- [30] J. Hofmann and W. Zwerger, Hydrodynamics of a superfluid smectic, *J. Stat. Mech.: Theory Exp.* **2021**, 033104.
- [31] B. P. Anderson and M. A. Kasevich, Macroscopic quantum interference from atomic tunnel arrays, *Science* **282**, 1686 (1998).
- [32] F. S. Cataliotti, S. Burger, C. Fort, P. Maddaloni, F. Minardi, A. Trombettoni, A. Smerzi, and M. Inguscio, Josephson junction arrays with Bose-Einstein condensates, *Science* **293**, 843 (2001).
- [33] D. Jaksch, C. Bruder, J. I. Cirac, C. W. Gardiner, and P. Zoller, Cold bosonic atoms in optical lattices, *Phys. Rev. Lett.* **81**, 3108 (1998).
- [34] P. Ilzhöfer, M. Sohmen, G. Durastante, C. Politi, A. Trautmann, G. Natale, G. Morpurgo, T. Giamarchi, L. Chomaz, M. J. Mark, and F. Ferlaino, Phase coherence in out-of-equilibrium supersolid states of ultracold dipolar atoms, *Nat. Phys.* **17**, 356 (2021).
- [35] C. Bühler, T. Ilg, and H. P. Büchler, Quantum fluctuations in one-dimensional supersolids, *Phys. Rev. Res.* **5**, 033092 (2023).
- [36] M. Kunimi, Y. Nagai, and Y. Kato, Josephson effects in one-dimensional supersolids, *Phys. Rev. B* **84**, 094521 (2011).
- [37] A. Smerzi, S. Fantoni, S. Giovanazzi, and S. R. Shenoy, Quantum coherent atomic tunneling between two trapped Bose-Einstein condensates, *Phys. Rev. Lett.* **79**, 4950 (1997).
- [38] A. M. Rey, K. Burnett, R. Roth, M. Edwards, C. J. Williams, and C. W. Clark, Bogoliubov approach to superfluidity of atoms in an optical lattice, *J. Phys. B* **36**, 825 (2003).
- [39] S. Paul and E. Tiesinga, Wannier functions using a discrete variable representation for optical lattices, *Phys. Rev. A* **94**, 033606 (2016).
- [40] P. B. Blakie and C. W. Clark, Wannier states and Bose-Hubbard parameters for 2D optical lattices, *J. Phys. B* **37**, 1391 (2004).